Supporting information

Enhanced Performance and Stability in DNA-Perovskite Heterostructure-based Solar Cells

Yuchen Hou[1], Kai Wang[1], Dong Yang[1], Yuanyuan Jiang[1], Neela Yennawar[2], Ke Wang[3], Mohan Sanghadasa,[4] Congcong Wu[1], Shashank Priya[1,3]

[1] Department of Materials Science and Engineering, Pennsylvania State University, University Park, PA 16802, United States

[2] Huck Institutes of the Life Sciences, Pennsylvania State University, University Park, PA 16802, United States

[3] Materials Research Institute, Pennsylvania State University, University Park, PA 16802, United States

[4] U.S. Army Combat Capabilities Development Command Aviation & Missile Center, Redstone Arsenal, Alabama 35898, United States

Correspondence and requests for materials should be addressed to C.W. (email: cuw635@psu.edu) and S.P. (email: sup103@psu.edu)

Materials and Methods

Materials Lead (II) iodide (PbI_2, 99.999%) was purchased from Acros Organics. Methylammonium iodide (MAI, purity >99.0%), 2. Hexadecyl trimethyl ammonium chloride (CTMA, purity >98.0 %), γ-butyrolactone (GBL, purity >99.0 %), acetonitrile (ACN, purity >99.8 %), methylamine solution (33 wt% in absolute ethanol), chlorobenzene (CB, purity >99.8 %), diethyl ether (purity >99.7 %), titanium isopropoxide (TTIP, 99.999 %) were purchased from Sigma-Aldrich. DNA (Deoxyribonucleic acid sodium salt from testes) with molecular mass of 1.3 x 10^6 Da (~2000 bp), %G-C content of 42.1 %, was purchased from Sigma-Aldrich. TiO_2 paste (18NR-T) was acquired from Dyesol. Ltd. 2,2',7,7'-Tetrakis[N,N-di(4-methoxyphenyl)amino]-9,9'-spirobifluorene (Spiro-OMeTAD, purity >99.99 %) was purchased from Luminescence Technology Corp. FTO glass was purchased from Nippon Sheet Glass Group. All the chemicals were used as purchased without further purification.

Preparation of DNA-CTMA solution In order to introduce hydrophilic DNA into perovskite solution, DNA was modified with CTMA. DNA solution was prepared by dissolving 60 mg DNA fibers into 10 mL DI water and stirred for 2 h. CTMA water solution with the same concentration was prepared in the same fashion. The CTMA water solution was slowly added into DNA water solution in a 1:1 volume ratio. The obtained solution containing DNA-CTMA complex was kept stirred overnight. The white DNA-CTMA precipitates were collected *via* vacuum filtration and dried in vacuum oven at 45 °C. The DNA-CTMA solution was prepared by dissolving different amount of DNA-CTMA powder into methylamine solution and stirred for 2 h.

Preparation of DNA-perovskite solution The $CH_3NH_3PbI_3$ ($MAPbI_3$) crystals were synthesized according to our previous work[1]. 120 mg black $MAPbI_3$ crystals were placed into a vial and exposed to CH_3NH_2 gases to form a yellow $MAPbI_3$ liquid intermedia. Then, 100 μL pure ACN and 100 μL DNA-CTMA solution was added to $MAPbI_3$ intermedia to form a DNA-perovskite solution. As a reference, the pristine perovskite solution was prepared by adding 100 μL pure ACN and 100 μL methylamine

solution into $MAPbI_3$ intermedia.

Solar cell device fabrication FTO glass substrates were cleaned ultrasonically by ethanol for 30 minutes. After drying by compressed air, the FTO glasses were treated by UV-ozone for 30 minutes. The compact TiO_2 layer was constructed by spin-coating TTIP solution onto FTO glass at 2000 rpm for 30 s, after which the glass is heated at 150 ℃ for 10 min. Mesoporous TiO_2 was then fabricated by spin-coating TiO_2 solution (18NR-T TiO_2 paste and ethanol in 2:7 weight ratio) at 6000 rpm for 30 s on compact TiO_2 layer, and subsequently the substrate was annealed at 500 ℃ for 30 minutes. The DNA-perovskite and pristine perovskite layer was made by spin-coating of perovskite solution on mesoporous TiO_2 layer at 4000 rpm for 35 s, followed by 100 ℃ annealing for 10 minutes. Spiro-OMeTAD solution was then spin-coated onto perovskite layer at 4000 rpm for 30 s. The spiro-OMeTAD solution was made by dissolving 48 mg of spiro-OMeTAD powder into 1 mL chlorobenzene containing 38 μL of 4-tert-butylpyridine and 26 μL of lithium bis(trifluoromethanesulfonyl)imide (500 mg/mL in acetonitrile). Finally, gold electrode (30 nm) was fabricated onto spiro-OMeTAD *via* thermal evaporation with an active cell area of 0.096 cm^2. For the fabrication of PSC device with DNA-CTMA film as HTL, DNA-CTMA solution (1 mg/mL in ethanol) was spin-coated onto perovskite layer at 4000 rpm for 30 s, followed by fabrication of 30 nm gold electrode.

Fabrication of hole-only device A hole-only device with FTO glass/PEDOT: PSS/perovskite/spiro-OMeTAD/Au structure was constructed. The PEDOT: PSS layer was spin-coated on the FTO glass at 4000 RPM for 30 s, followed by annealing at 150 ℃ for 10 minutes. The perovskite layer and spiro-OMeTAD layer were then spin-coated onto PEDOT:PSS. Finally, 100 nm of gold electrode was deposited on the top. The J-V response of the hole-only device was measured by a Keithley 2400 source meter at room temperature in the dark.

Characterization High-resolution TEM images of perovskite crystals were obtained by a FEI dual aberration corrected Titan^3 G2 60-300 scanning/transmission electron microscope (S/TEM) operating at an accelerating voltage of 80 kV. The energy

dispersive x-ray (EDS) elemental mapping was performed with a SuperX EDS system under STEM mode. Electron energy loss spectroscopy (EELS) measurements were performed using a GIF quantum 965 system (dual EELS mode). For TEM sample preparation, the perovskite film was deposited onto glass, and then perovskite crystals were gently scratched off by holey carbon film on copper grid from film surface. SEM images of perovskite film surface and solar cell cross-section were obtained by a Merlin LEO 1530 field-emission scanning electron microscope. The surface topology and surface potential were measured by a Bruker Icon II instrument operating at PeakForce kelvin probe mode using a Pt-Ir coated Si conductive tip. Fourier-transform infrared (FTIR) spectra were collected on a Bruker Vertex V70 spectrometer by measuring Brewster's angle transmission. Photoluminescence (PL) spectra were obtained by an Edinburgh Instrument FLS1000 fluorescence spectrometer at room temperature with an excitation irradiation of 506 nm by Xenon lamp. For Time-resolved photoluminescence (TRPL) spectroscopy measurement, a picosecond pulsed diode laser at 506 nm was used as excitation source and signals were collected by a TCSPC detector. UV-Vis absorption spectra of perovskite film were collected by a Hitachi UH4150 spectrometer at room temperature. Photovoltaic performance of solar cell device was evaluated by measuring the J-V characteristics of unencapsulated device in the air under simulated AM 1.5G light irradiation generated by a 450W xenon lamp (Oriel Sol 2A ABA), which was calibrated by a standard reference silicon cell covered with KG5 filter glass. The J-V curves were recorded by a Keithley 2400 source meter with scan rate of 0.1 V. s^{-1} and scan step of 0.02 V. Incident photon-to-electron efficiency (IPCE) was measured by a Newport QuantX-300 quantum efficiency measurement system at ambient condition without encapsulation. Electrochemical impedance spectroscopy (EIS) of the solar cell device was measured in the dark at V_{oc} bias using a 660E Electrochemical workstation (CHI Instruments Inc.) in the frequency range of 0.01-10^6 Hz. For Mott-Schottky analysis, impedance response of the solar cell device is measured from -0.2 V to 1.2 V at 20k Hz.

Supplemental Figures and Tables

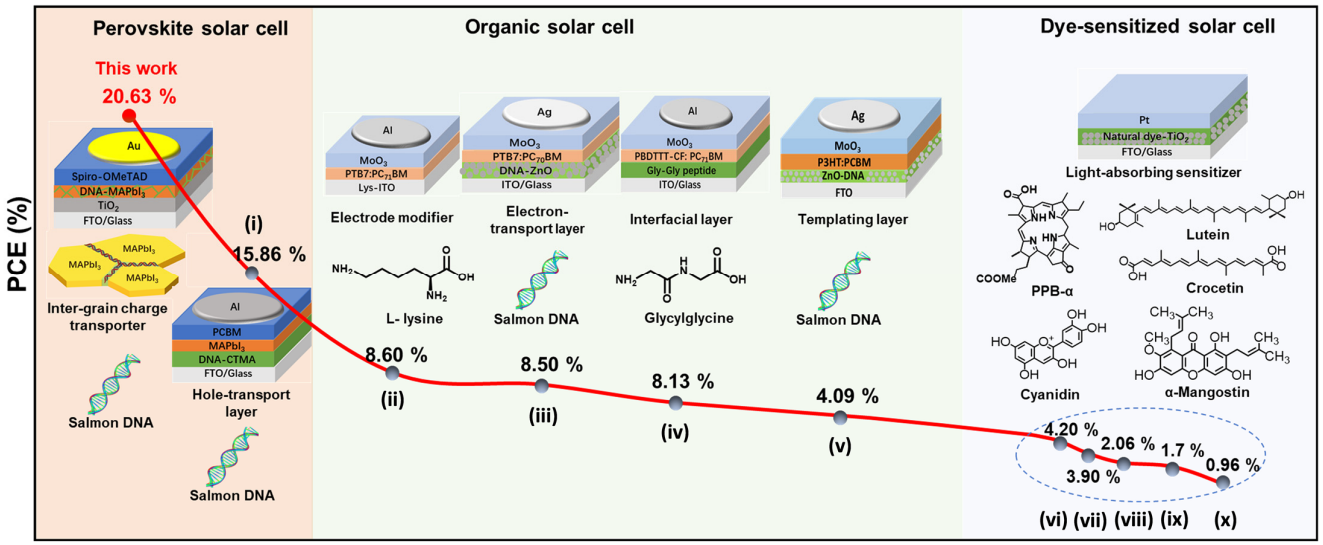

Supplemental figure S1. Summary of bio-photovoltaic devices performance based in various solar cell classes. (i) Yusoff et al., EPFL. Ref. [11] (ii) Deng et al., HIT. Ref. [7] (iii) Dajar et al., URTV. Ref. [9] (iv) Nie et al. HIT. Ref. [6] (v) Toschi et al., ISM-CNR. Ref. [10] (vi) & (vii) Wang et al., KGU. Ref. [2] (viii) Henning et al., UoB. Ref. [3]. (ix) Calogero et al., CNR-IPCF. Ref. [5] (x) Kumara et al., UBD. Ref. [4]

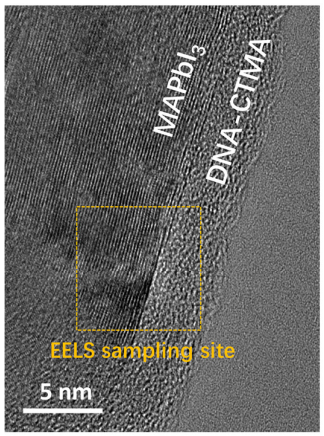

Supplemental figure S2. HRTEM image of the perovskite/DNA interface. Electron beam is focused on the interface area marked by yellow box for EELS measurement.

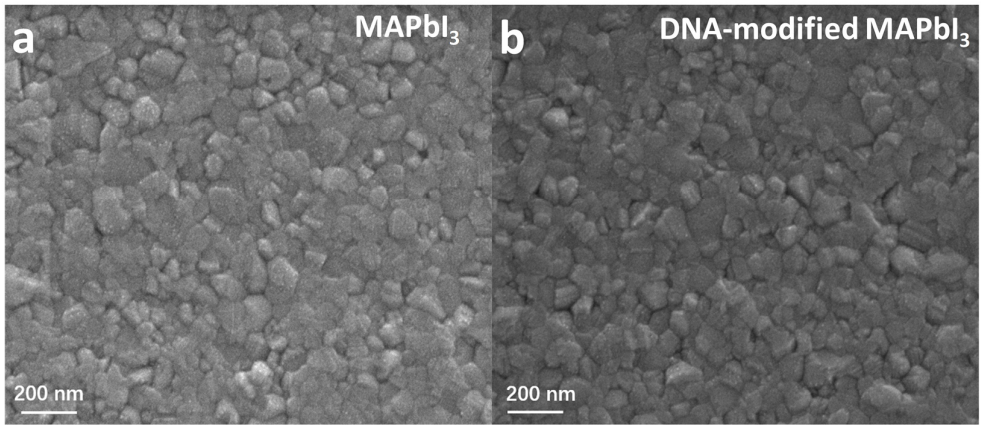

Supplemental figure S3. SEM images of (a) Pristine $MAPbI_3$ film (b) DNA-modified $MAPbI_3$ film.

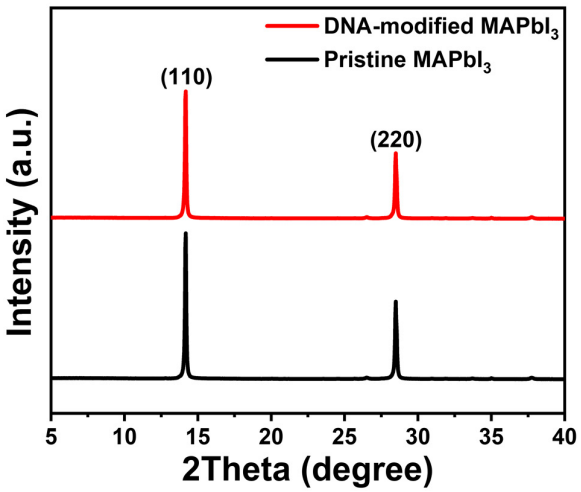

Supplemental figure S4. XRD patterns of pristine and DNA-modified $MAPbI_3$ films

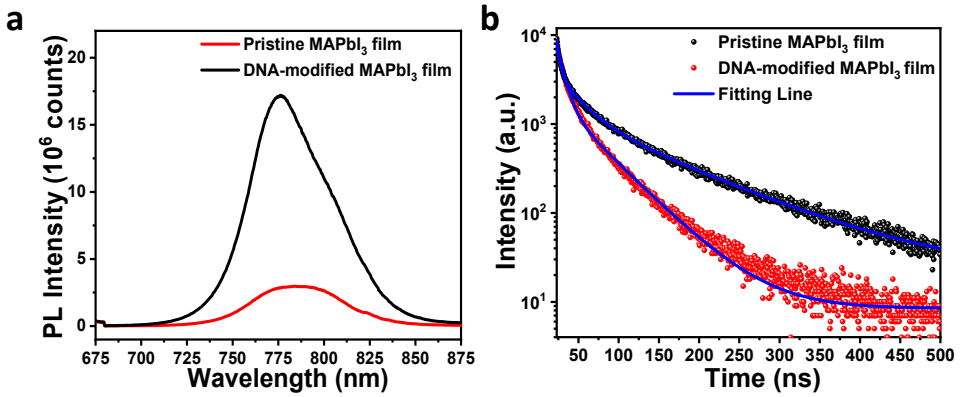

Supplemental figure S5. (a) Steady-state PL spectra and (b) Time-resolved PL spectra of pristine $MAPbI_3$ perovskite film and DNA-modified $MAPbI_3$ film.

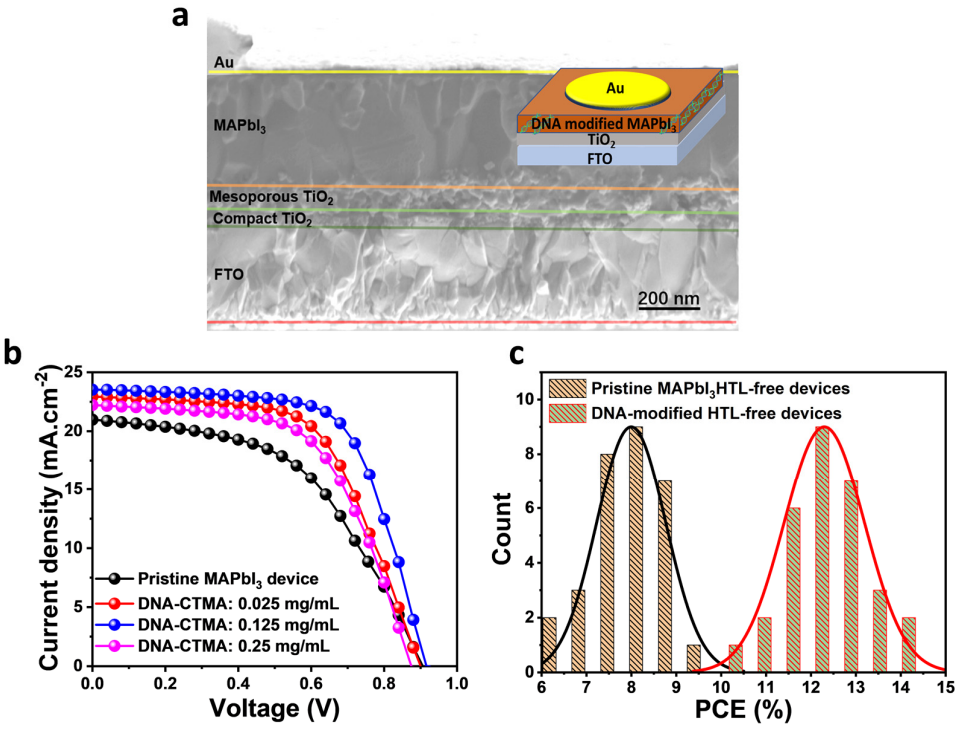

Supplemental figure S6. Performance of hole extraction layer (HTL)-free device based on pristine $MAPbI_3$ and DNA-modified $MAPbI_3$. (a) Schematic of HTL-free structured solar cell (top) Cross-section SEM image of device (bottom). (b) J-V curves of HTL-free devices under simulated sunlight illumination. (c) Statistics of PCE distribution histogram of 30 pristine and DNA-modified devices with optimal DNA concentration of 0.125 mg/mL (HF D-0.125).

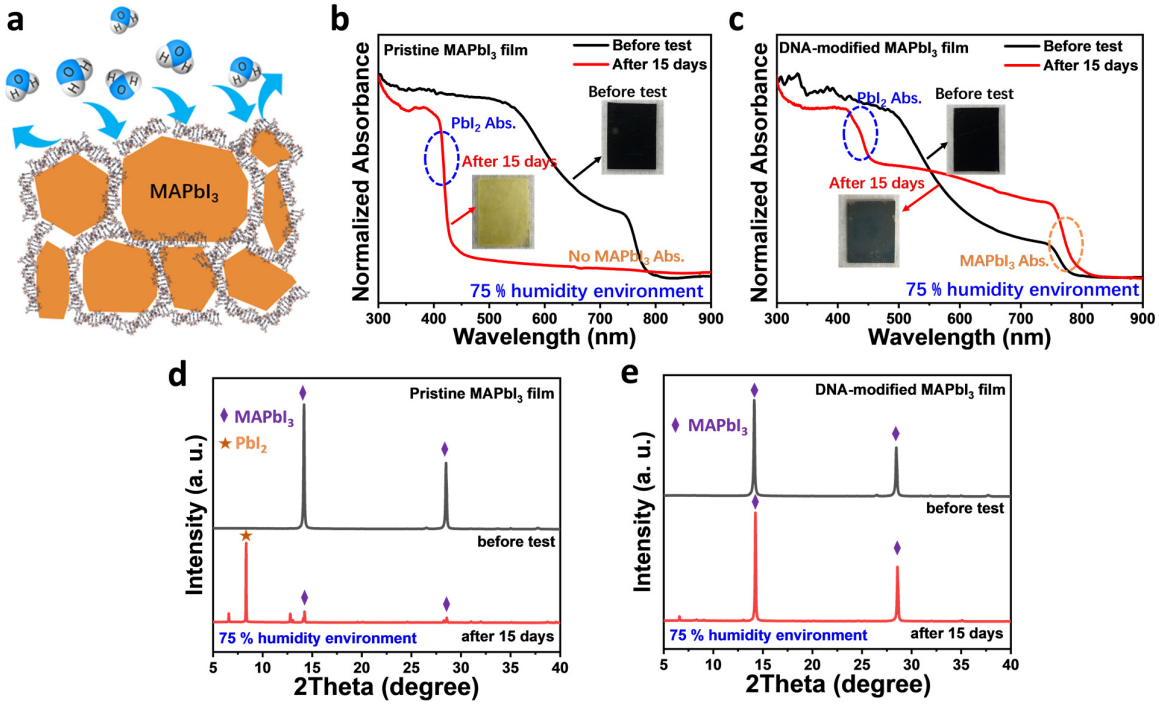

Supplemental figure S7. Stability of the $MAPbI_3$ perovskite film in extreme humidity condition. (a) Schematic illustration of DNA-CTMA among the grain boundaries of $MAPbI_3$ serves as barrier to block moisture attack. (b)-(c): UV-Vis absorption spectra of (b) pristine $MAPbI_3$ and (c) DNA-modified $MAPbI_3$ before test and after 15 days in a sealed chamber with controlled humidity of 75 %. In the pristine film all $MAPbI_3$ was degraded into PbI_2 as observed from presence of absorption edge of PbI_2 and absence of $MAPbI_3$ absorption edge. In contrast, there are still strong absorption from $MAPbI_3$ in DNA-modified film, indicating $MAPbI_3$ is well protected. Inset are photo images of perovskite films before and after 15 days of exposure to extreme humidity, showing a clear contrast of moisture stability between pristine and DNA-modified perovskite film. (d)-(e) XRD of (d) pristine $MAPbI_3$ and (e) DNA-modified $MAPbI_3$ film before and after exposure to humidity, showing majority of the pristine $MAPbI_3$ was degraded to PbI_2 while DNA-modified $MAPbI_3$ didn't show significant sign of degradation.

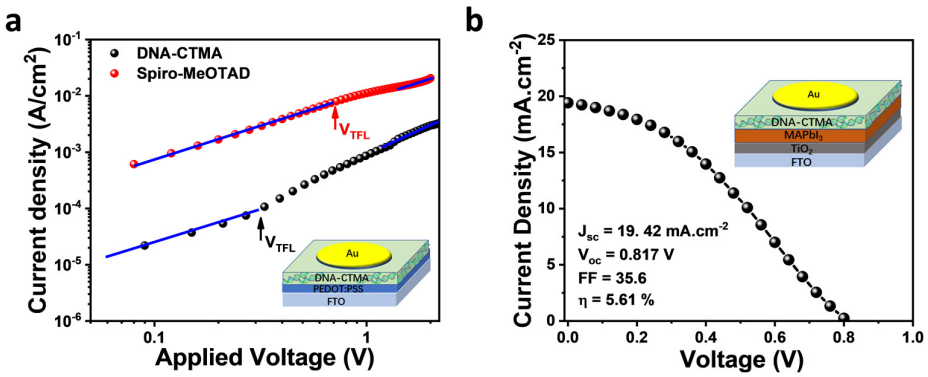

Supplemental figure S8. (a) J-V characteristics of hole-only device based on DNA-CTMA and spiro-OMeTAD film fitted by SCLC model. (b) J-V response and photovoltaic parameters of PSC device under simulated sunlight using DNA-CTMA as hole transport layer. Insert shows the corresponding device structure

Table S1 Stretching mode and corresponding assignment for different samples in FTIR spectra		
Samples	**Peak assignment**	**Wavenumber (cm^{-1})**
DNA-CTMA	N-H, C=N, CH_3 stretching	3000-3600
	C=N stretching in imines, oximes	1696
	C=O stretching in amide	1650
	C=C vibration in imidazole ring	1478
	Asymmetric and symmetric stretching of PO_2^-	1238, 1070
	Sugar-phosphate group vibration	800-900
	Asymmetric and symmetric stretching of CH_2 in CTMA	2928, 2852
$MAPbI_3$	CH_3-NH_3 rock	917
	C-N stretching	961
	Asymmetric and symmetric NH_3^+ bend	1582, 1460
	Asymmetric and symmetric NH_3^+ stretch	3174, 3124

Table S2 Parameters of TRPL measurement for pristine and DNA-modified $MAPbI_3$ thin film					
Samples	τ_{ave} [ns]	τ_1 [ns]	τ_2 [ns]	% of τ_1	% of τ_2
Pristine $MAPbI_3$	82.78	8.56	84.89	22.10	77.90
DNA-modified $MAPbI_3$	44.06	9.00	48.51	40.82	59.18

Table S3 Hole extraction layer-free device performance with $MAPbI_3$ film doped with different concentration of DNA-CTMA				
HTL-free device	J_{sc} [$mA.cm^{-2}$]	V_{oc} [V]	FF [%]	PCE [%]
Reference	20.98	0.906	50.4	9.59
HF D-0.025	22.93	0.900	59.4	12.26
HF D-0.125	23.52	0.916	65.2	14.05
HF D-0.25	22.22	0.845	59.1	11.49

Supporting Information Note 1

Table S4 summarized performance of example bio-photovoltaic devices based on various solar cell structures. In dye-sensitized solar cells (DSSCs), natural dyes extracted from various plants were used as light-harvesting sensitizer to generate charge carriers. Several dye pigments employed for DDSCs were shown as examples[2-5]. The highest power conversion efficiency for bio-photovoltaic built upon DSSC was ~4.20 %[2]. Bio-photovoltaics were also investigated based on organic solar cell (OSC) structure. Nie et al. incorporated an ultrathin interfacial layer of peptide on ITO electrode which attained a PCE of 8.13 % in inverted OSC device[6]. Deng et al. used amino acid to tune the work function of ITO electrode and achieved an improved PCE of 8.60 %.[7] DNA thin film was incorporate as electron transport layer (ETL) in organic solar cell by Dajar et al. and achieved PCE of 4.94 %[8]. In another study, ZnO film coated by DNA was utilized as ETL for enhancing the electron transport property of organic solar cell. PCE of the device reached an improved value of 8.5 % compared with the device made using pristine ZnO[9]. In a recent study by Toschi et al.[10], DNA was also used as a templating layer inserting between the ZnO (EEL) and organic photoabsorber in OSC. The DNA interlayer was found to introduce a different long-range structure in the P3HT polymer compared with the case without DNA. It was found the resulting structure led to larger delocalization of photogenerated excitons, which facilitate exciton disassociation into free polarons. As a result, PCE of the DNA-integrated device reached 4.09 %, which is 21 % enhancement compared with the device without DNA interlayer. There is very limited study of bio-photovoltaics in perovskite solar cell. Recently, DNA-CTMA was employed as hole-transport layer by Yusoff et al. and a PCE of 15.86 % was achieved[11].

Table S4 Bio photovoltaics based on different solar cell architecture							
Bio-photovoltaic type	**Biomaterial**	**Role of biomaterial**	J_{sc}[mA cm^{-2}]	V_{oc}[V]	FF[%]	η [%]	**Ref.**
Perovskite solar cell	Salmon DNA	Inter-grain charge transporter	23.46	1.12	78.9	20.63	This work
	Salmon DNA	Hole-transport layer	20.85	1.04	73.1	15.86	[11]
Organic solar cell	L- lysine	Electrode modifier	17.1	0.75	67	8.6	[7]
	Salmon DNA	Electron-transport layer	18.95	0.72	62.53	8.5	[9]
	Glycylglycine	Interfacial layer	17.69	0.73	63	8.13	[6]
	Salmon DNA	Electron-transport layer	14.08	0.72	49.7	4.94	[8]
	Salmon DNA	Templating layer	12.58	0.59	61.83	4.10	[10]
Dye sensitized solar cell	PBB-α	Natural dye sensitizer	13.7	0.53	0.58	4.2	[2]
	Lutein		11.8	0.55	0.60	3.9	[2]
	Crocetin		8.8	0.39	0.60	2.06	[3]
	Cyanidin		9.5	0.43	0.37	1.70	[5]
	α-Mangostin		6.25	0.35	0.44	0.96	[4]

Supporting Information 2

Figure S9 shows a model of DNA molecule binding to surface of perovskite. For the model generation, the $MAPbI_3$ structure was imported from Cambridge Structural Database (CSD), and coordinates for an ideal B-DNA was generated using the Coot software. As seen from the model in every turn of major and minor grooves of DNA molecule there are six PO_4 groups which are close enough to interact with Pb atoms exposed on the surface of $MAPbI_3$ crystal. The six Pb-PO_4 interactions can be divided into two parts (marked in two red boxes in Figure S9a), each consists of three Pb-PO_4 bonds. Figure S9b shows the three PO_4 groups I, II, and III marked with cyan box. To better visualize the spatial configuration of these three PO_4 groups, a schematic of the model viewing from y-axis direction was presented in Figure S9c. As seen the interspace of PO_4 groups along the DNA strand well aligned with the interspace distance of Pb atoms on perovskite surface, which enables three strong Pb-PO_4 electrostatic bonds. These Pb-PO_4 bonds act like “anchors” to tightly bind the DNA molecule on the perovskite surface. In addition, neighboring perovskite crystals could be glued together on different faces of the DNA helical backbone resulting in the DNA pulling the perovskite grains to pack tightly and reducing trap sites.

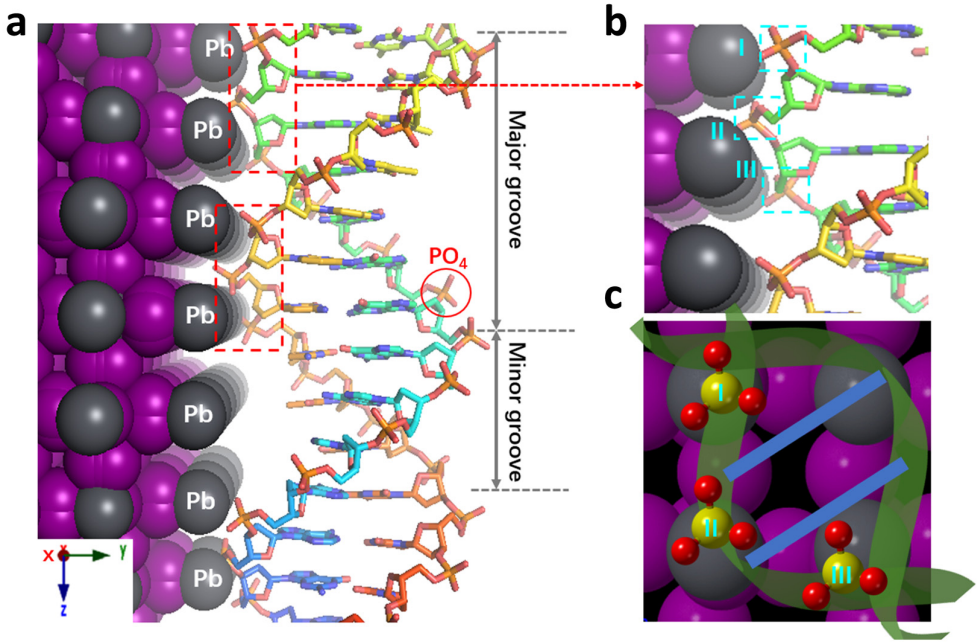

Supplemental figure S9. (a) Schematic illustration of DNA binding to perovskite surface. There are six Pb-PO_4 bonding interactions (marked in two red boxes) in every repeating major and minor grooves of DNA chain. (b) Enlarged view of one box containing three PO_4 groups (marked with I, II and III) binding to Pb on perovskite surface. (c) Spatial configuration of the three PO_4 groups viewing from the y-axis direction showing good alignment of PO_4 group with Pb atoms.

Supporting Information 3

Fermi level of perovskite film can be calculated based on the contact potential difference measured in KPFM characteriztaion[12]:

$$CPD = \emptyset_{tip} - \emptyset_{sample}$$

Φ_{tip} and Φ_{sample} represents the work function of AFM tip and sample surface, respectively. Φ_{tip} can be calculated by measuring the potential difference between Pt/Ir-coated tip and a known substrate such as standard highly oriented pyrolytic graphite (HOPG). Work function of HOPG is 4.6 V[13]. Therefore, the fermi level of sample, FL_{sample}, is simply:

$$FL_{sample} = e\left[-4.6 + (CPD_{sample} - CPD_{HOPG})\right]$$

where e is the elementary charge, CPD_{sample} and CPD_{HOPG} is the measured contact potential difference of tip with respect to sample and standard HOPG, respectively. Figure S10a shows the CPD mapping of HOPG in a 0.2 x 0.2 μm area, and Figure S10b shows the CPD profile of $MAPbI_3$, DNA-modified $MAPbI_3$ and HOPG film. CPD_{HOPG} was ~466 mV, therefore Fermi level of pristine and DNA-modified $MAPbI_3$ were determined to be ~-4.907 eV and -5.013 eV, respectively.

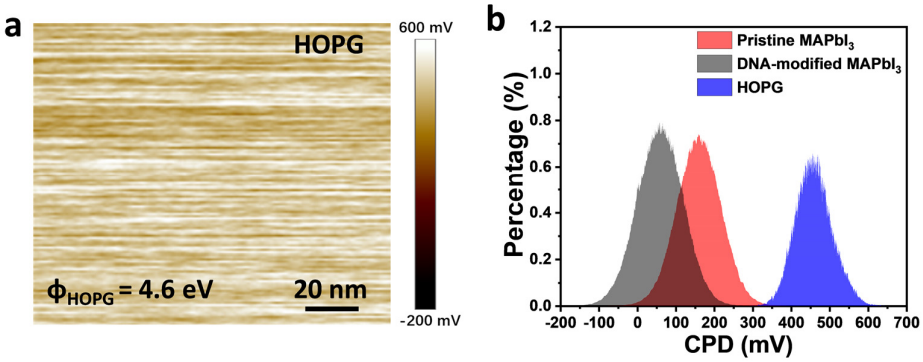

Supplemental figure S10. (a) Surface potential mapping of HOPG surface. (b) Contact potential difference (CPD) profile of $MAPbI_3$, DNA-modified $MAPbI_3$ and HOPG film.

Supporting Information 4

Carrier concentration change in solar cell device upon DNA-integration was characterized by measuring the capacitance response of device under applied voltage ($1/C^2$-V curve) in the dark condition. Measurement is performed with a CHI 660 E instrument at 20k Hz from -0.2 V to 1.2 V. The active electrode area was 0.096 cm^{-2}. The slope (k) of the linear region in the $1/C^2$-V curve can be fitted by Mott-Schottky relation[14-15]:

$$k = \frac{2}{eN\varepsilon_r\varepsilon_0}$$

, where e is the elementary charge, N is the concentration of major charge carriers, ε_r is the relative permeability of $MAPbI_3$, which is 32, and ε_0 is the vacuum permeability. Figure S11 shows the measured $1/C^2$-V plot of solar cell device based on pristine and DNA-modified $MAPbI_3$. The negative slope indicated that major carriers are holes, and hole concentration of $MAPbI_3$ is calculated to be 3.65 x 10^{15} cm^{-3} which increases to 7.38 x 10^{15} cm^{-3} after DNA incorporation, suggesting a p-type doping effect by DNA molecules.

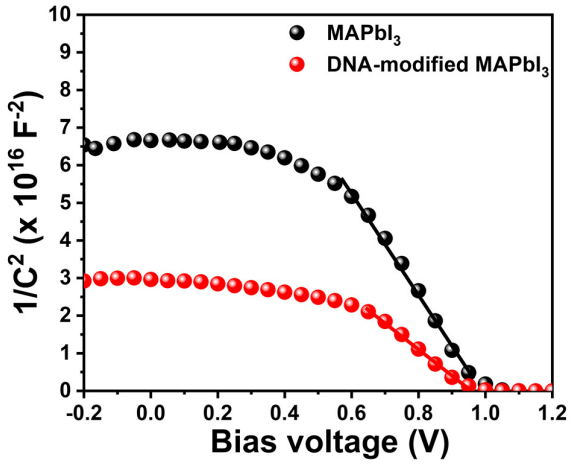

Supplemental figure S11. Carrier density characterization. Mott-Schottky plot (relationship between capacitance of device and applied voltage in the dark) of solar cell devices fabricated by pristine and DNA-modified $MAPbI_3$.

Reference

1. Wu, C.; Li, H.; Yan, Y.; Chi, B.; Felice, K. M.; Moore, R. B.; Magill, B. A.; Mudiyanselage, R. R.; Khodaparast, G. A.; Sanghadasa, M., Highly-Stable Organo-Lead Halide Perovskites Synthesized Through Green Self-Assembly Process. *Solar RRL* **2018,** *2* (6), 1800052.
2. Wang, X. F.; Matsuda, A.; Koyama, Y.; Nagae, H.; Sasaki, S. i.; Tamiaki, H.; Wada, Y., Effects of plant carotenoid spacers on the performance of a dye-sensitized solar cell using a chlorophyll derivative: enhancement of photocurrent determined by one electron-oxidation potential of each carotenoid. *Chemical physics letters* **2006,** *423* (4-6), 470-475.
3. Henning, A.; Günzburger, G.; Jöhr, R.; Rosenwaks, Y.; Bozic-Weber, B.; Housecroft, C. E.; Constable, E. C.; Meyer, E.; Glatzel, T., Kelvin probe force microscopy of nanocrystalline TiO2 photoelectrodes. *Beilstein journal of nanotechnology* **2013,** *4* (1), 418-428.
4. Kumara, N.; Ekanayake, P.; Lim, A.; Liew, L. Y. C.; Iskandar, M.; Ming, L. C.; Senadeera, G., Layered co-sensitization for enhancement of conversion efficiency of natural dye sensitized solar cells. *Journal of alloys and compounds* **2013,** *581*, 186-191.
5. Calogero, G.; Di Marco, G.; Cazzanti, S.; Caramori, S.; Argazzi, R.; Di Carlo, A.; Bignozzi, C. A., Efficient dye-sensitized solar cells using red turnip and purple wild sicilian prickly pear fruits. *International journal of molecular sciences* **2010,** *11* (1), 254-267.
6. Nie, R.; Li, A.; Deng, X., Environmentally friendly biomaterials as an interfacial layer for highly efficient and air-stable inverted organic solar cells. *Journal of Materials Chemistry A* **2014,** *2* (19), 6734-6739.
7. Deng, X.; Nie, R.; Li, A.; Wei, H.; Zheng, S.; Huang, W.; Mo, Y.; Su, Y.; Wang, Q.; Li, Y.; Tang, J.; Xu, J.; Wong, K. y., Ultra-Low Work Function Transparent Electrodes Achieved by Naturally Occurring Biomaterials for Organic Optoelectronic Devices. *Advanced Materials Interfaces* **2014,** *1* (7), 1400215.
8. Dagar, J.; Scarselli, M.; De Crescenzi, M.; Brown, T. M., Solar cells incorporating water/alcohol-soluble electron-extracting DNA nanolayers. *ACS Energy Letters* **2016,** *1* (3), 510-515.
9. Dagar, J.; Scavia, G.; Scarselli, M.; Destri, S.; De Crescenzi, M.; Brown, T. M., Coating ZnO nanoparticle films with DNA nanolayers for enhancing the electron extracting properties and performance of polymer solar cells. *Nanoscale* **2017,** *9* (48), 19031-19038.
10. Toschi, F.; Catone, D.; O'Keeffe, P.; Paladini, A.; Turchini, S.; Dagar, J.; Brown, T. M., Enhanced charge separation efficiency in DNA templated polymer solar cells. *Advanced Functional Materials* **2018,** *28* (26), 1707126.
11. Yusoff, A. R. b. M.; Kim, J.; Jang, J.; Nazeeruddin, M. K., New Horizons for Perovskite Solar Cells Employing DNA-CTMA as the Hole-Transporting Material. *ChemSusChem* **2016,** *9* (13), 1736-1742.
12. Melitz, W.; Shen, J.; Lee, S.; Lee, J. S.; Kummel, A. C.; Droopad, R.; Yu, E. T., Scanning tunneling spectroscopy and Kelvin probe force microscopy investigation of Fermi energy level pinning mechanism on InAs and InGaAs clean surfaces. *Journal of Applied Physics* **2010,** *108* (2), 023711.
13. Yang, D.; Yang, R.; Wang, K.; Wu, C.; Zhu, X.; Feng, J.; Ren, X.; Fang, G.; Priya, S.; Liu, S. F., High efficiency planar-type perovskite solar cells with negligible hysteresis using EDTA-complexed SnO 2. *Nature communications* **2018,** *9* (1), 3239.
14. Chen, B. X.; Rao, H. S.; Li, W. G.; Xu, Y. F.; Chen, H. Y.; Kuang, D. B.; Su, C. Y., Achieving high-performance planar perovskite solar cell with Nb-doped TiO_2 compact layer by enhanced electron injection and efficient charge extraction. *Journal of Materials Chemistry A* **2016,** *4* (15), 5647-5653.
15. Zhang, Y.; Zhou, H.; Seifter, J.; Ying, L.; Mikhailovsky, A.; Heeger, A. J.; Bazan, G. C.; Nguyen, T. Q., Molecular doping enhances photoconductivity in polymer bulk heterojunction solar cells. *Advanced*

Materials **2013,** *25* (48), 7038-7044.